

Calcium Directly Regulates Phosphatidylinositol 4,5-Bisphosphate Headgroup Conformation and Recognition

Eva Bilkova,^{†,‡,¶} Roman Pleskot,^{§,||,¶} Sami Rissanen,^{⊥,¶} Simou Sun,^{#,⊗,¶} Aleksander Czogalla,^{†,∇} Lukasz Cwiklik,^{&,§} Tomasz Róg,^{⊥,○} Ilpo Vattulainen,^{⊥,○,◆} Paul S. Cremer,^{*,#,⊗} Pavel Jungwirth,^{*,§,⊥} and Ünal Coskun^{*,†,‡}

[†]Paul Langerhans Institute Dresden of the Helmholtz Zentrum München at the University Hospital and Faculty of Medicine Carl Gustav Carus of TU Dresden, Technische Universität Dresden, Fetscher Strasse 74, 01307 Dresden, Germany

[‡]German Center for Diabetes Research (DZD e.V.), Ingolstädter Landstraße 1, 85764 Neuherberg, Germany

[§]Institute of Organic Chemistry and Biochemistry, Academy of Sciences of the Czech Republic, Flemingovo náměstí 2, 16610 Prague 6, Czech Republic

^{||}Institute of Experimental Botany, Academy of Sciences of the Czech Republic, v.v.i., Rozvojová 263, 16502 Prague 6, Czech Republic

[⊥]Department of Physics, Tampere University of Technology, P.O. Box 692, FI-33101 Tampere, Finland

[#]Department of Chemistry and [⊗]Department of Biochemistry and Molecular Biology, Penn State University, University Park, Pennsylvania 16801, United States

[∇]Laboratory of Cytobiochemistry, Faculty of Biotechnology, University of Wrocław, Joliot-Curie 14a, 50-383 Wrocław, Poland

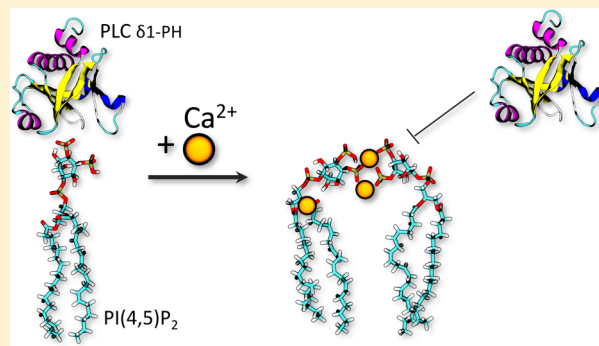
[&]J. Heyrovský Institute of Physical Chemistry, Academy of Sciences of the Czech Republic, v.v.i., Dolejškova 3, 18223 Prague 8, Czech Republic

[○]Department of Physics, University of Helsinki, P.O. Box 64, FI-00014, Helsinki, Finland

[◆]MEMPHYS— Center for Biomembrane Physics, University of Southern Denmark, DK-5230 Odense, Denmark

Supporting Information

ABSTRACT: The orchestrated recognition of phosphoinositides and concomitant intracellular release of Ca^{2+} is pivotal to almost every aspect of cellular processes, including membrane homeostasis, cell division and growth, vesicle trafficking, as well as secretion. Although Ca^{2+} is known to directly impact phosphoinositide clustering, little is known about the molecular basis for this or its significance in cellular signaling. Here, we study the direct interaction of Ca^{2+} with phosphatidylinositol 4,5-bisphosphate ($\text{PI}(4,5)\text{P}_2$), the main lipid marker of the plasma membrane. Electrokinetic potential measurements of $\text{PI}(4,5)\text{P}_2$ containing liposomes reveal that Ca^{2+} as well as Mg^{2+} reduce the zeta potential of liposomes to nearly background levels of pure phosphatidylcholine membranes. Strikingly, lipid recognition by the default $\text{PI}(4,5)\text{P}_2$ lipid sensor, phospholipase C delta 1 pleckstrin homology domain (PLC $\delta 1$ -PH), is completely inhibited in the presence of Ca^{2+} , while Mg^{2+} has no effect with 100 nm liposomes and modest effect with giant unilamellar vesicles. Consistent with biochemical data, vibrational sum frequency spectroscopy and atomistic molecular dynamics simulations reveal how Ca^{2+} binding to the $\text{PI}(4,5)\text{P}_2$ headgroup and carbonyl regions leads to confined lipid headgroup tilting and conformational rearrangements. We rationalize these findings by the ability of calcium to block a highly specific interaction between PLC $\delta 1$ -PH and $\text{PI}(4,5)\text{P}_2$, encoded within the conformational properties of the lipid itself. Our studies demonstrate the possibility that switchable phosphoinositide conformational states can serve as lipid recognition and controlled cell signaling mechanisms.



INTRODUCTION

Cell signaling pathways are largely organized via a specific recruitment of signaling effector proteins to their target membranes and a confined release of calcium ions. The quintessential example of this is the action of phospholipase C (PLC) that binds and hydrolyzes phosphatidylinositol 4,5-bisphosphate ($\text{PI}(4,5)\text{P}_2$) in the plasma membrane to

diacylglycerol (DAG) and the water-soluble inositol 1,4,5-trisphosphate (IP_3), the latter inducing the release of Ca^{2+} from the endoplasmic reticulum (ER) into the cytosol.¹ Another prominent example is synaptotagmin-1, the main Ca^{2+} sensor of

Received: November 14, 2016

Published: February 8, 2017

neuronal exocytosis in the presynaptic axon terminal. Synaptotagmin-1 binding to PI(4,5)P₂ directly amplifies protein cooperativity and thus sensitivity to Ca²⁺ by a factor of >40. This mutual interplay is a critical step in neurotransmitter release.²

PI(4,5)P₂ is enriched in the inner leaflet of the plasma membrane^{3,4} and constitutes around 1% of the total anionic phospholipid content in cellular membranes.⁵ In comparison with other phospholipids, it contains a rather bulky phosphorylated inositol headgroup with a negative charge ranging from $-3 e$ to $-5 e$, depending on the pH and the presence of proteins or ions.⁶ PI(4,5)P₂ and other negatively charged lipids in the cytosolic leaflet are constantly exposed to divalent cations. In resting cells, the free cytosolic Ca²⁺ concentration is approximately 100 nM.^{7,8} The cytosolic concentration of Ca²⁺ upon cell signaling has been reported to span a wide range from 0.5 μ M to several hundred μ M, with a half-life of 500 μ s to 26 ms.^{9–14} Ca²⁺ influx primarily originates from internal stores within the endoplasmic/sarcoplasmic reticulum or from specialized channels within the plasma membrane providing an essentially infinite supply of extracellular calcium.⁹ In all cases, Ca²⁺ is delivered as brief transients, forming microdomains at the membrane site of influx,¹⁰ and thus, local concentrations of Ca²⁺ can be expected to exceed cytosolic concentrations by orders of magnitude.¹⁵ Meanwhile, unlike Ca²⁺, the levels of free, cytosolic Mg²⁺ are maintained within a fairly narrow concentration range of 0.25–1 mM.^{16,17} Interestingly, calcium but not magnesium ions have been ascribed a strong propensity to promote the formation of PI(4,5)P₂ clusters as demonstrated in several studies, primarily by using monolayer techniques.^{18–22}

While the overall effects of divalent cations, including calcium, on PI(4,5)P₂ lateral organization have been intensely studied, the mechanism of Ca²⁺ and PI(4,5)P₂ interactions at the molecular level remain unclear. Experiments with pure PI(4,5)P₂ monolayers have suggested partial dehydration of both Ca²⁺ and PI(4,5)P₂ upon interaction with each other,²³ triggering an electron density increase in the PI(4,5)P₂ headgroup region as well as acyl chain region thickening.²⁴ Interactions between PI(4,5)P₂ and Ca²⁺ have also been studied computationally. These studies, however, have typically focused on single PI(4,5)P₂ molecules²⁵ or used simplified coarse-grained models¹⁹ that lack sufficient details to deal with specific chemical features of phosphatidylinositides.

Herein, we combine protein–lipid binding assays and spectroscopic experiments with atomistic molecular dynamics (MD) simulations employing refined state-of-the-art force fields to unravel the functional and structural consequences of the interplay between Ca²⁺ and PI(4,5)P₂. Our data indicate a hitherto undiscovered role and mechanism for Ca²⁺ in cellular signaling, namely the direct organization of the phosphoinositide headgroup conformation and the selective recognition thereof by the pleckstrin homology (PH) domain of PLC δ 1, the canonical PI(4,5)P₂ sensor.

RESULTS AND DISCUSSION

Protein–Lipid Binding Assays. To determine the equilibrium dissociation constants (K_D) for divalent cation/PI(4,5)P₂ interaction, we employed a simple fluorescent assay using a supported lipid bilayer platform^{26–28} containing 5 mol % of PI(4,5)P₂ (for details, see the Supporting Information). Significantly, the K_D values differed by less than a factor of 2, with a K_D of 0.6 ± 0.2 mM for Ca²⁺ compared to 1.2 ± 0.2 mM

for Mg²⁺ (Figure S1). We therefore decided to use a cation concentration of 1 mM for all follow-up experiments, matching the free Mg²⁺ concentration in the cytosol. In order to systematically study the effects of Ca²⁺ on PI(4,5)P₂, we produced 100 nm diameter large unilamellar vesicles (LUVs), facilitating the control of membrane lipid composition and properties. For quality control and physicochemical characterization, all preparations were first subjected to thin layer chromatography (TLC), dynamic light scattering (DLS), and zeta potential measurements (Figure S2). Having the opposite charge of PI(4,5)P₂, it is not surprising that Ca²⁺ and Mg²⁺ equally reduce the zeta potential of POPC liposomes containing 5 mol % of PI(4,5)P₂, the former being described previously.²⁹ In fact, the presence of either cation attenuates the electrokinetic potential of the membrane down to the level of POPC alone (Figure S2c).

Because of its extraordinary stereospecificity, the PLC δ 1-PH domain is widely used as the canonical reporter for cellular PI(4,5)P₂ levels at the plasma membrane as well as with *in vitro* assays.^{30–34} We therefore used recombinant PLC δ 1-PH domain to follow PI(4,5)P₂ binding to synthetic liposomes. Size-exclusion chromatography and DLS confirmed that the purified PLC δ 1-PH domain (Figure S3a,b) was monomeric in solution, even in the presence of Ca²⁺ and Mg²⁺ (Figure S3c,d). Next, we performed liposome flotation assays to follow PLC δ 1-PH binding efficiency to POPC/PI(4,5)P₂ vesicles. Interestingly, preincubation with 1 mM Ca²⁺ but not 1 mM Mg²⁺ fully inhibited liposome binding (Figure 1a,b). Moreover, PLC δ 1-PH did not bind to pure POPC liposomes, highlighting its specificity to PI(4,5)P₂.

Circular dichroism (CD) spectroscopy excluded a direct effect for cations on the secondary structure of the protein (Figure S3e,f). As such, although Ca²⁺ and Mg²⁺ bind to PI(4,5)P₂ with comparable K_D values and reduce electrokinetic membrane properties in an equal manner, only Ca²⁺ was capable of inhibiting PLC δ 1-PH binding. This indicates that PI(4,5)P₂ recognition by proteins cannot be solely based on electrostatic interactions.

Because a concentration of 1 mM Ca²⁺ corresponds to twice its K_D for PI(4,5)P₂ interaction, we performed additional flotation assays with lower Ca²⁺ concentrations. Here, a significant reduction in protein binding could be observed already at a concentration of 0.6 mM Ca²⁺ (Figure S4). In this context, recent data by Milovanovic and colleagues show that Ca²⁺ but not Mg²⁺ promotes syntaxin-1/PI(4,5)P₂ domain formation by an underlying mechanism in which Ca²⁺ clusters PI(4,5)P₂ and syntaxin-1 independently from each other. Moreover, Ca²⁺ acts as a charge bridge that merges multiple syntaxin-1/PI(4,5)P₂ clusters into larger domains. Also here, Ca²⁺ was found to be effective at a concentration of 0.5 mM while even 1 mM Mg²⁺ had no effect.³⁵

Ca²⁺ binding to membranes has been recently reported to increase with high curvature.³⁶ We therefore additionally followed the binding of monomeric ECFP-PLC δ 1-PH fusion protein to giant unilamellar vesicles (GUVs) (Figure 1c). Despite limited control over membrane lipid composition at the individual GUV level,³⁷ GUVs provide the most appropriate synthetic approach for flat and freestanding bilayer systems. In this system, the presence of 1 mM Ca²⁺ drastically reduced ECFP-PLC δ 1-PH binding (Figure 1d and Figure S5), demonstrating the robustness of the observed effect, irrespective of membrane curvature. Magnesium, however, also reduced ECFP-PLC δ 1-PH domain binding, halfway

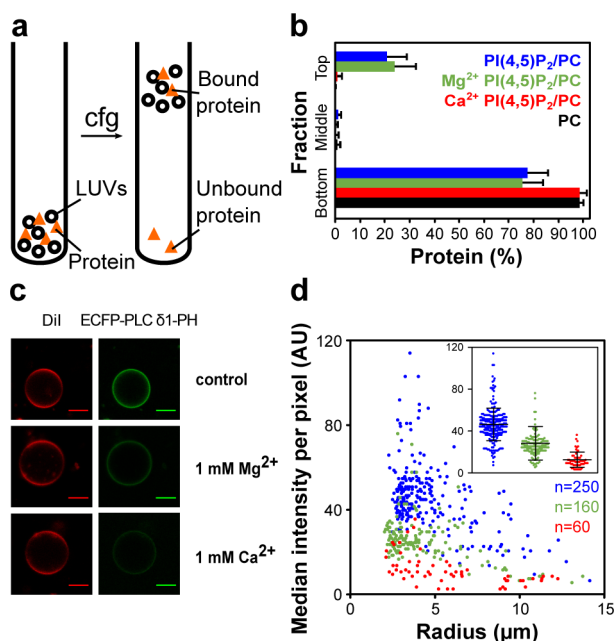


Figure 1. (a) Setup of the LUV flotation assay. (b) PLC $\delta 1$ -PH binding to LUVs with POPC/PI(4,5) P_2 (95/5 mol %). Error bars are standard deviations of three independent experiments. (c) LUVs after ECFP-PLC $\delta 1$ -PH addition (green) and Dil as membrane marker (red). The scale bar corresponds to 10 μm . (d) The distribution of median ECFP-PLC $\delta 1$ -PH intensity per pixel of individual LUVs and different sizes of control (blue) and after preincubation with 1 mM Mg^{2+} (green) or Ca^{2+} (red) (data from two additional independent experiments are provided in Figure S5). Each dot represents a single LUV. The number of analyzed LUVs is indicated in the respective color. The median intensity values with mean and standard deviation are depicted in the inset. The Mann–Whitney test was used as significance test (p value < 0.0001 for all cases).

toward the Ca^{2+} effect. To understand this result, it is important to note that liposome flotation experiments with proteins are nonequilibrium assays because much of the protein stays in the bottom of the tube. At the same time, cation concentrations remain constant, leading to an additional stoichiometric shift. By contrast, protein binding in the LUV experiment is at equilibrium and binding events are quantified at the individual LUV level.

Vibrational Sum Frequency Spectroscopy. To analyze the molecular basis for the cation specificity, vibrational sum frequency spectroscopy (VSFS) was employed to study the effects of Ca^{2+} and Mg^{2+} on pure PI(4,5) P_2 monolayers at the air/water interface. The spectra were recorded over frequency ranges corresponding to the headgroup and acyl-chain portions of the lipid molecules and included the adjacent interfacial water structure.

We present VSFS spectra from the inositol ring and phosphate regions of PI(4,5) P_2 in the absence and presence of 1 mM Ca^{2+} and Mg^{2+} (Figure 2a, detailed peak assignments in Figure S6 and Table S1). In the absence of cations in the subphase, both the inositol ring vibrations and the phosphate stretches were rather weak (black data points). This is because of a relatively disordered arrangement of the PI(4,5) P_2 headgroups adopted in a pure buffer with a wide range of tilt angles relative to the surface normal. With 1 mM Ca^{2+} , however, the inositol ring signal (961 cm^{-1} and 1012 cm^{-1} peaks from the C–C and C–O coupled vibrations, respectively)³⁸ increased substantially (red data points). In

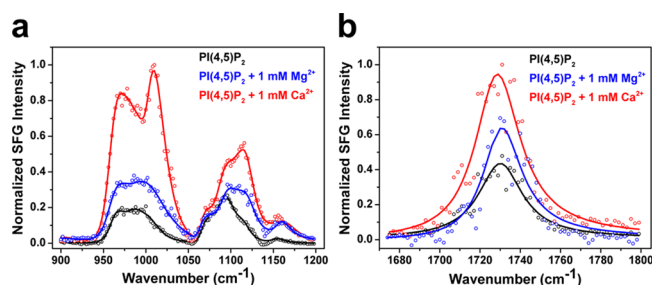


Figure 2. VSFS spectra of (a) the inositol ring and phosphate regions and (b) the carbonyl C=O symmetric stretch region of PI(4,5) P_2 on a buffer subphase (black spectra) containing 1 mM MgCl_2 (blue spectra) or 1 mM CaCl_2 (red spectrum) at a surface pressure of 17 mN/m. The open circles represent VSFS data points, and the solid lines are fits to the data. All spectra were taken with the ssp polarization combination. Spectra of the same data offset along the y-axis are provided in Figure S7. Details of monolayer preparation and images are provided in Figure S14.

fact, the resonances showed 2.7- and 3.6-fold increases, respectively, in oscillator strength (Table S1). These changes reflect both reorientation of the inositol rings and a narrowing of their orientational distribution upon cation binding. Significantly, the changes were not nearly as strong upon the addition of 1 mM Mg^{2+} (blue data points). In that case, the oscillator strength of the inositol ring vibrations was increased by only a factor of 1.5 and 2.1, respectively. Such results indicated that Ca^{2+} rigidified the configuration of the PI(4,5) P_2 headgroups much more effectively than Mg^{2+} .

In addition to the inositol ring modes, the phosphate peaks (e.g., symPO_3^{2-} at 982 cm^{-1} , symPO_2^- at 1086 cm^{-1} , asyPO_3^{2-} at 1115 cm^{-1} , asyPO_2^- at 1154 cm^{-1} , detailed assignments in Figure S6 and Table S1) also showed a substantial intensity increase upon the introduction of Ca^{2+} to the subphase. This indicates a strong net orientation and/or ordering of the headgroup phosphates upon Ca^{2+} binding. It should be noted that Ca^{2+} binding may help to deprotonate the second monoesterified phosphate,²⁵ which would prompt additional changes in the spectra beyond those related to ordering and tilt angle. Moreover, upon the addition of Ca^{2+} , the symmetric PO_3^{2-} stretch exhibited a relatively large 20 cm^{-1} blue shift, while the asymmetric PO_3^{2-} and PO_2^- stretches shifted by 6 cm^{-1} and 8 cm^{-1} , respectively (Table S1). The shifts of both PO_3^{2-} peaks are consistent with phosphate dehydration upon cation binding and/or a symmetry change of the C_{3v} point group.^{39,40} The shift of the asymmetric PO_2^- peak also suggests headgroup phosphate dehydration upon Ca^{2+} binding.^{40–42}

The spectral change brought about by 1 mM Mg^{2+} in the phosphate region was much less pronounced overall compared to that with 1 mM Ca^{2+} . The difference in the interactions of Ca^{2+} and Mg^{2+} with phosphate could be explained at least in part by different dehydration penalties for these two cations. It has been suggested that Ca^{2+} binding to phosphate groups is favored because Ca^{2+} is more easily dehydrated than Mg^{2+} .²³ This difference in the hydration shell chemistry may, in turn, act to disfavor the bridging of the inositol rings of PI(4,5) P_2 , which would weaken the ordering effect of Mg^{2+} .

In addition to phosphate and inositol resonances, VSFS spectra were also obtained in the carbonyl C=O symmetric stretch (1730 cm^{-1})⁴³ region before and after addition of 1 mM CaCl_2 or MgCl_2 (Figure 2b). Again, Ca^{2+} showed a more prominent effect on the PI(4,5) P_2 than Mg^{2+} . In fact, a 1.6-fold

increase in the oscillator strength of this peak was observed upon binding of Ca^{2+} , while only a 1.3-fold increase was found for Mg^{2+} (Table S2). This oscillator strength increase should correspond to a backbone ordering effect, thus helping to reinforce a more rigid configuration of the headgroup inositol rings. Ordering of the lipid acyl chains was also observed (Figure S8 and Table S3).⁴⁴

Taken together, the changes in the VSFS spectra provide strong experimental evidence for distinct conformational changes within the lipid headgroup region in the presence of Ca^{2+} , but less with Mg^{2+} . Such results should be important for the PLC $\delta 1$ -PH domain selectivity of $\text{PI}(4,5)\text{P}_2$ found above with liposomes and GUVs.

Atomistic Molecular Dynamics Simulations. With the aim of obtaining mechanistic insights into the effects of Ca^{2+} and Mg^{2+} on $\text{PI}(4,5)\text{P}_2$ molecules at a molecular level, we employed atomistic MD simulations. In order to reduce methodological bias, we used two all-atom force fields (OPLS-AA and CHARMM36) as well as the united-atom force field from Berger (Table S4).^{45–47} Importantly, to further account for electronic polarization effects of charged groups in a mean field manner, for Ca^{2+} interacting with $\text{PI}(4,5)\text{P}_2$ phosphates we also employed the recently developed electronic continuum correction with rescaling (ECCR) method.⁴⁸ This, to a large extent, dampens the unrealistically high ion pairing found when employing nonpolarizable force fields.⁴⁸ It is particularly useful in the present case where strong electronic polarization can be expected in the vicinity of multiple-charged moieties.

We generated multiple sets of 1 μs long trajectories for different initial $\text{PI}(4,5)\text{P}_2$ distributions prior to and after the addition of Ca^{2+} or Mg^{2+} . For all simulations, consistently with all force fields used, we find that Ca^{2+} interacts with $\text{PI}(4,5)\text{P}_2$ and has a pronounced effect on the lipid headgroup orientation (Figure 3 and Figures S9 and S13). Moreover, control simulations with Mg^{2+} showed that the effects induced by magnesium are much weaker than those induced by calcium for all simulations (Figure 3c,d and S1), in full agreement with experiments.

The addition of Ca^{2+} or Mg^{2+} immediately leads to a significant reduction of the area per lipid (Figure S10 and Table S5). This macroscopic effect is in agreement with lateral condensation of the $\text{PI}(4,5)\text{P}_2$ -containing monolayers by Ca^{2+} ^{20,22–24} and our VSFS analysis of the CH stretches (Figure S8). At the microscopic level, we found that each $\text{PI}(4,5)\text{P}_2$ molecule binds on average 1.6–3.1 Ca^{2+} molecules, depending on the force field that is employed (Table S5). This is consistent with the water peak spectral changes, which show that each lipid molecule binds more than two Ca^{2+} ions (Figure S8). Ca^{2+} binds mostly to the phosphate groups at positions 4 and 5, but it also penetrates deeper into the lipid bilayer to interact with the carbonyl groups (Figure S11). Ca^{2+} binding to the lipid carbonyl group is consistent with the VSFS data in the carbonyl stretch region, as documented herein (Figure 2b) and elsewhere.^{49–53} In agreement with previously published computational and experimental results,^{24,50} we observed that Ca^{2+} increases the order parameters of the $\text{PI}(4,5)\text{P}_2$ acyl chains (Figure S12). The acyl chain ordering is also fully in line with the effects observed in the VSFS spectra (Figure S8).

The most prominent feature observed by simulations is a pronounced headgroup reorientation, primarily caused by the ability of Ca^{2+} to bridge two $\text{PI}(4,5)\text{P}_2$ headgroups (Figure 3a,b). This result was found regardless of which force field was

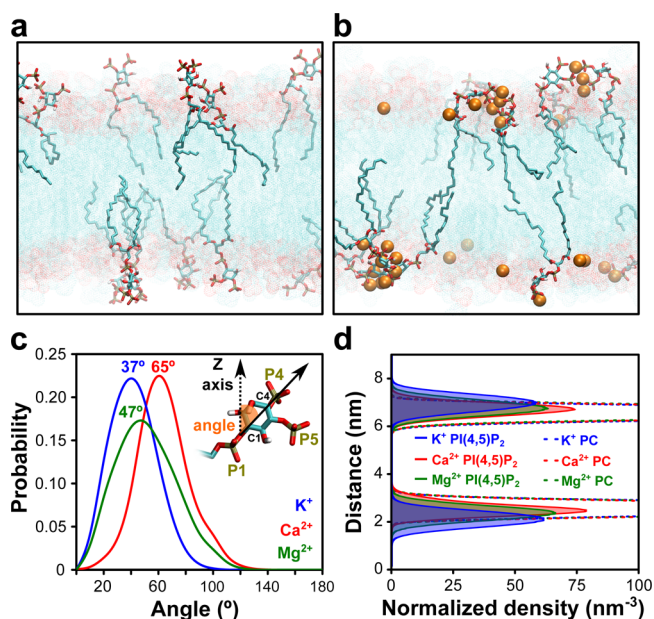


Figure 3. Snapshots from MD simulations of the lipid bilayer taken at 1 μs (a) without and (b) with Ca^{2+} . (c) Tilt angle distribution of the $\text{PI}(4,5)\text{P}_2$ headgroup and (d) density profiles of lipid headgroups without (blue) and with Mg^{2+} (green) or Ca^{2+} (red). Numbers in (c) represent mean tilt angles for each system. Here, only the results of the Berger force field simulations are presented. Additional force field simulations with similar outcomes can be found in the [Supporting Information](#).

used. To quantitatively analyze the headgroup reorientation, we monitored the tilt angle between the C1–C4 atoms of the $\text{PI}(4,5)\text{P}_2$ inositol ring and the bilayer normal. The average tilt angle in the control simulation without Ca^{2+} was in the range of 35–41°, depending on the employed force field. This result is in agreement with previously published MD studies.^{54–56} In the presence of Ca^{2+} ions, however, the average tilt angle significantly increased for all of the force fields up to 65° (Figure 3c and Figures S9 and S13). Simulations thus consistently showed bending of the $\text{PI}(4,5)\text{P}_2$ headgroup toward the plane of the bilayer and away from bulk water (Table S5). Moreover, consistent with a narrowing of the inositol ring's distribution as indicated by VSFS results above (Figure 2a), Ca^{2+} slowed $\text{PI}(4,5)\text{P}_2$ headgroup rotational diffusion as revealed by the rotational correlation function (Figure S9e). The Ca^{2+} effect was also manifested in the density profiles (Figure 3d), where the location of the $\text{PI}(4,5)\text{P}_2$ headgroups shifted in the presence of calcium toward the bilayer center. Moreover, Ca^{2+} significantly decreased the solvent accessible surface area of $\text{PI}(4,5)\text{P}_2$, which correlated with a reduced average number of hydrogen bonds between the $\text{PI}(4,5)\text{P}_2$ headgroups and water molecules (Table S5). These data also match the experimentally observed partial dehydration of $\text{PI}(4,5)\text{P}_2$ in the presence of Ca^{2+} as measured here by VSFS and elsewhere.²³

The charge state of $\text{PI}(4,5)\text{P}_2$ in lipid membranes is highly sensitive to the cellular pH and the presence of proteins and ions.^{6,57} By using not only the default parametrization (CHARMM36 and OPLS-AA) but also the ECCR corrected charges for the ions and $\text{PI}(4,5)\text{P}_2$ phosphate groups (Berger, OPLS-AA), we were able to assess the potential effects of the lipid charge state. Namely, the charge used for $\text{PI}(4,5)\text{P}_2$ varied from -3.75 to -5 , depending on the particular force field (for

more details, see the SI). Reassuringly, we found semi-quantitatively the same effect of Ca^{2+} on the PI(4,5) P_2 tilt angle with Ca^{2+} in all the systems which were tested. This indicates that under the conditions of these investigations the protonation state of PI(4,5) P_2 was not particularly critical for the observed effects.

CONCLUSION

By means of protein–lipid binding assays and spectroscopic experiments, together with atomistic MD simulations, we have unraveled and characterized in molecular detail the pronounced effect of Ca^{2+} on PI(4,5) P_2 headgroup presentation. First, we confirmed the previously observed increase of the PI(4,5) P_2 acyl chain order and PI(4,5) P_2 cluster formation,^{18–21} as evidenced here by VSFG spectroscopy and MD simulations. Second, we characterized at the molecular level the interactions of Ca^{2+} with PI(4,5) P_2 headgroup phosphates, as well as the more deeply seated carbonyl groups. We observed the hitherto unrecognized consequences of Ca^{2+} binding for PI(4,5) P_2 at the molecular level. Namely, we observed a dramatic change in the PI(4,5) P_2 headgroup tilt angle. By means of liposome flotation and GUV binding assays, we show that Ca^{2+} has a strong propensity to render the PI(4,5) P_2 headgroup invisible to the PLC- $\delta 1$ PH domain.

Our data lead to the plausible conjecture that the calcium-induced switching of phosphoinositide conformational states may serve as a potential cellular mechanism for lipid recognition and thus play a decisive role in cell signaling and membrane trafficking. A systematic correlation of kinetics and curvature sensitivities at the nanoscale *in vitro*⁵⁸ will be key to understanding the general applicability of our data to other proteins and to different endomembranes.

ASSOCIATED CONTENT

Supporting Information

The Supporting Information is available free of charge on the ACS Publications website at DOI: 10.1021/jacs.6b11760.

Detailed materials and methods, additional VSFS spectra, computational and experimental controls (PDF)

AUTHOR INFORMATION

Corresponding Authors

*pscl1@psu.edu

*pavel.jungwirth@uochb.cas.cz

*coskun@plid.de

ORCID

Tomasz Róg: 0000-0001-6765-7013

Ilpo Vattulainen: 0000-0001-7408-3214

Paul S. Cremer: 0000-0002-8524-0438

Pavel Jungwirth: 0000-0002-6892-3288

Ünal Coskun: 0000-0003-4375-3144

Author Contributions

[¶]E.B., R.P., S.R., and S.S. contributed equally.

Notes

The authors declare no competing financial interest.

ACKNOWLEDGMENTS

We thank Milena Stephan, André Nadler, and Alf Honigmann (Max Planck Institute of Molecular Cell Biology and Genetics) for support with GUV image quantification and GUV production protocol; Josef Lazar (C4Sys research infra-

structure) for advice on background correction in Fiji; and the light-microscopy facility of the BIOTEC/CRTD at TU Dresden for providing excellent microscopy support and maintenance. We thank Michal Grzybek for skillful experimental advice and support. P.J. thanks the Academy of Finland for the FiDiPro Award. We acknowledge generous computational resources made available by CSC-IT Centre for Science (Espoo, Finland) and the High-Performance Computing Center of the TU Dresden. Financial support was provided by the Deutsche Forschungsgemeinschaft (DFG) “Transregio 83” (Grant No. TRR83 TP18 (Ü.C., A.C., E.B.)), the German Federal Ministry of Education and Research grant to the German Center for Diabetes Research (DZD e.V.) (Ü.C.), the Academy of Finland (Center of Excellence program) (I.V., T.R., S.R.), the European Research Council (Advanced Grant CROWDED-PRO-LIPIDS) (I.V.), a FEBS Short-Term Fellowship (S.R.), the Graduate School program of Tampere University of Technology and Alfred Kordelin Foundation (S.R.), the Polish Ministry of Science and Higher Education (Iuventus Plus 2015–2016 project IP2014 007373) (A.C.), the Dresden International Graduate School for Biomedicine and Bioengineering, granted by the DFG (GS97) (E.B.), the Czech Science Foundation GACR 13-19073S (R.P.), 16-01074S (P.J.), and 17-06792S (L.C.), the National Science Foundation (CHE-1413307 (P.S.C.)), and the Office of Naval Research (N00014-14-1-0792 (P.S.C.)).

REFERENCES

- (1) Putney, J. W.; Tomita, T. *Adv. Biol. Regul.* **2012**, *52* (1), 152–64.
- (2) van den Bogaart, G.; Meyenberg, K.; Diederichsen, U.; Jahn, R. *J. Biol. Chem.* **2012**, *287* (20), 16447–53.
- (3) McLaughlin, S.; Wang, J.; Gambhir, A.; Murray, D. *Annu. Rev. Biophys. Biomol. Struct.* **2002**, *31*, 151–75.
- (4) Di Paolo, G.; De Camilli, P. *Nature* **2006**, *443* (7112), 651–7.
- (5) Nasuhoglu, C.; Feng, S.; Mao, J.; Yamamoto, M.; Yin, H. L.; Earnest, S.; Barylko, B.; Albanesi, J. P.; Hilgemann, D. W. *Anal. Biochem.* **2002**, *301* (2), 243–54.
- (6) Wang, Y. H.; Slochower, D. R.; Janmey, P. A. *Chem. Phys. Lipids* **2014**, *182*, 38–51.
- (7) Clapham, D. E. *Cell* **2007**, *131* (6), 1047–58.
- (8) Usachev, Y. M.; Marchenko, S. M.; Sage, S. O. *J. Physiol.* **1995**, *489*, 309–17.
- (9) Berridge, M. J. *J. Physiol.* **1997**, *499*, 291–306.
- (10) Berridge, M. J. *Cell Calcium* **2006**, *40* (5–6), 405–12.
- (11) Heidelberger, R.; Heinemann, C.; Neher, E.; Matthews, G. *Nature* **1994**, *371* (6497), 513–5.
- (12) Llinas, R.; Sugimori, M.; Silver, R. B. *Science* **1992**, *256* (5057), 677–9.
- (13) Tengholm, A.; Gylfe, E. *Mol. Cell. Endocrinol.* **2009**, *297* (1–2), 58–72.
- (14) Ammala, C.; Eliasson, L.; Bokvist, K.; Larsson, O.; Ashcroft, F. M.; Rorsman, P. *J. Physiol.* **1993**, *472*, 665–88.
- (15) Parekh, A. B. *J. Physiol.* **2008**, *586* (13), 3043–54.
- (16) Grubbs, R. D. *BioMetals* **2002**, *15* (3), 251–9.
- (17) Fujise, H.; Cruz, P.; Reo, N. V.; Lauf, P. K. *Biochim. Biophys. Acta, Mol. Cell Res.* **1991**, *1094* (1), 51–54.
- (18) Carvalho, K.; Ramos, L.; Roy, C.; Picart, C. *Biophys. J.* **2008**, *95* (9), 4348–60.
- (19) Ellenbroek, W. G.; Wang, Y. H.; Christian, D. A.; Discher, D. E.; Janmey, P. A.; Liu, A. J. *Biophys. J.* **2011**, *101* (9), 2178–84.
- (20) Levental, I.; Christian, D. A.; Wang, Y. H.; Madara, J. J.; Discher, D. E.; Janmey, P. A. *Biochemistry* **2009**, *48* (34), 8241–8.
- (21) Sarmiento, M. J.; Coutinho, A.; Fedorov, A.; Prieto, M.; Fernandes, F. *Biochim. Biophys. Acta, Biomembr.* **2014**, *1838* (3), 822–30.

- (22) Levental, I.; Cebers, A.; Janmey, P. A. *J. Am. Chem. Soc.* **2008**, *130* (28), 9025–30.
- (23) Wang, Y. H.; Collins, A.; Guo, L.; Smith-Dupont, K. B.; Gai, F.; Svitkina, T.; Janmey, P. A. *J. Am. Chem. Soc.* **2012**, *134* (7), 3387–95.
- (24) Graber, Z. T.; Wang, W.; Singh, G.; Kuzmenko, I.; Vaknin, D.; Kooijman, E. E. *RSC Adv.* **2015**, *5* (129), 106536–106542.
- (25) Slochow, D. R.; Huwe, P. J.; Radhakrishnan, R.; Janmey, P. A. *J. Phys. Chem. B* **2013**, *117* (28), 8322–9.
- (26) Jung, H.; Robison, A. D.; Cremer, P. S. *J. Am. Chem. Soc.* **2009**, *131* (3), 1006–14.
- (27) Huang, D.; Zhao, T.; Xu, W.; Yang, T.; Cremer, P. S. *Anal. Chem.* **2013**, *85* (21), 10240–8.
- (28) Robison, A. D.; Sun, S.; Poyton, M. F.; Johnson, G. A.; Pellois, J. P.; Jungwirth, P.; Vazdar, M.; Cremer, P. S. *J. Phys. Chem. B* **2016**, *120* (35), 9287–96.
- (29) Toner, M.; Vaio, G.; McLaughlin, A.; McLaughlin, S. *Biochemistry* **1988**, *27* (19), 7435–43.
- (30) Balla, T.; Varnai, P. *Sci. Signaling* **2002**, *2002* (125), pl3.
- (31) Garcia, P.; Gupta, R.; Shah, S.; Morris, A. J.; Rudge, S. A.; Scarlata, S.; Petrova, V.; McLaughlin, S.; Rebecchi, M. J. *Biochemistry* **1995**, *34* (49), 16228–34.
- (32) Saliba, A. E.; Vonkova, I.; Ceschia, S.; Findlay, G. M.; Maeda, K.; Tischer, C.; Deghou, S.; van Noort, V.; Bork, P.; Pawson, T.; Ellenberg, J.; Gavin, A. C. *Nat. Methods* **2013**, *11* (1), 47–50.
- (33) Lemmon, M. A.; Ferguson, K. M.; O'Brien, R.; Sigler, P. B.; Schlessinger, J. *Proc. Natl. Acad. Sci. U. S. A.* **1995**, *92* (23), 10472–6.
- (34) Lemmon, M. A. *Nat. Rev. Mol. Cell Biol.* **2008**, *9* (2), 99–111.
- (35) Milovanovic, D.; Platen, M.; Junius, M.; Diederichsen, U.; Schaap, I. A.; Honigsmann, A.; Jahn, R.; van den Bogaart, G. *J. Biol. Chem.* **2016**, *291* (15), 7868–76.
- (36) Magarkar, A.; Jurkiewicz, P.; Allolio, C.; Hof, M.; Jungwirth, P. *J. Phys. Chem. Lett.* **2017**, *8* (2), 518–523.
- (37) Czogalla, A.; Grzybek, M.; Jones, W.; Coskun, U. *Biochim. Biophys. Acta, Mol. Cell Biol. Lipids* **2014**, *1841* (8), 1049–59.
- (38) Isbrandt, L. R.; Oertel, R. P. *J. Am. Chem. Soc.* **1980**, *102* (9), 3144–3148.
- (39) Laroche, G.; Dufourc, E. J.; Dufourcq, J.; Pezolet, M. *Biochemistry* **1991**, *30* (12), 3105–14.
- (40) Casillas-Ituarte, N. N.; Chen, X.; Castada, H.; Allen, H. C. *J. Phys. Chem. B* **2010**, *114* (29), 9485–95.
- (41) Levinson, N. M.; Bolte, E. E.; Miller, C. S.; Corcelli, S. A.; Boxer, S. G. *J. Am. Chem. Soc.* **2011**, *133* (34), 13236–9.
- (42) Flach, C. R.; Brauner, J. W.; Mendelsohn, R. *Biophys. J.* **1993**, *65* (5), 1994–2001.
- (43) Rzeznicka, I.; Sovago, M.; Backus, E. H.; Bonn, M.; Yamada, T.; Kobayashi, T.; Kawai, M. *Langmuir* **2010**, *26* (20), 16055–62.
- (44) Gurau, M. C.; Lim, S. M.; Castellana, E. T.; Albertorio, F.; Kataoka, S.; Cremer, P. S. *J. Am. Chem. Soc.* **2004**, *126* (34), 10522–3.
- (45) Klauda, J. B.; Venable, R. M.; Freites, J. A.; O'Connor, J. W.; Tobias, D. J.; Mondragon-Ramirez, C.; Vorobyov, I.; MacKerell, A. D., Jr.; Pastor, R. W. *J. Phys. Chem. B* **2010**, *114* (23), 7830–43.
- (46) Jorgensen, W. L.; Chandrasekhar, J.; Madura, J. D.; Impey, R. W.; Klein, M. L. *J. Chem. Phys.* **1983**, *79* (2), 926–935.
- (47) Berger, O.; Edholm, O.; Jahnig, F. *Biophys. J.* **1997**, *72* (5), 2002–13.
- (48) Kohagen, M.; Pluharova, E.; Mason, P. E.; Jungwirth, P. *J. Phys. Chem. Lett.* **2015**, *6* (9), 1563–7.
- (49) Porasso, R. D.; Lopez Cascales, J. J. *Colloids Surf., B* **2009**, *73* (1), 42–50.
- (50) Bockmann, R. A.; Grubmuller, H. *Angew. Chem., Int. Ed.* **2004**, *43* (8), 1021–4.
- (51) Magarkar, A.; Rog, T.; Bunker, A. *J. Phys. Chem. C* **2014**, *118* (33), 19444–19449.
- (52) Binder, H.; Zschornig, O. *Chem. Phys. Lipids* **2002**, *115* (1–2), 39–61.
- (53) Melcrova, A.; Pokorna, S.; Pullanchery, S.; Kohagen, M.; Jurkiewicz, P.; Hof, M.; Jungwirth, P.; Cremer, P. S.; Cwiklik, L. *Sci. Rep.* **2016**, *6*, 38035.
- (54) Li, Z.; Venable, R. M.; Rogers, L. A.; Murray, D.; Pastor, R. W. *Biophys. J.* **2009**, *97* (1), 155–63.
- (55) Lupyán, D.; Mezei, M.; Logothetis, D. E.; Osman, R. *Biophys. J.* **2010**, *98* (2), 240–7.
- (56) Wu, E. L.; Qi, Y.; Song, K. C.; Klauda, J. B.; Im, W. *J. Phys. Chem. B* **2014**, *118* (16), 4315–25.
- (57) Graber, Z. T.; Gericke, A.; Kooijman, E. E. *Chem. Phys. Lipids* **2014**, *182*, 62–72.
- (58) Mathiasen, S.; Christensen, S. M.; Fung, J. J.; Rasmussen, S. G. F.; Fay, J. F.; Jorgensen, S. K.; Veshaguri, S.; Farrens, D. L.; Kiskowski, M.; Kobilka, B.; Stamou, D. *Nat. Methods* **2014**, *11* (9), 931–934.